Wind and Structures, Vol. 12, No. 1 (2009) 77-88
DOI: http://dx.doi.org/10.12989/was.2009.12.1.077

Wind pressure measurements on a cube subjected to pulsed impinging jet flow

M.S. Mason

School of Civil Engineering, University of Sydney, Sydney NSW, Australia

D.L. James*

Department of Mechanical Engineering, Texas Tech University, Lubbock TX, USA

C.W. Letchford

School of Engineering, University of Tasmania, Hobart, Tasmania, Australia
(Received June 26, 2008, Accepted December 17, 2008)

Abstract. A pulsed impinging jet is used to simulate the gust front of a thunderstorm downburst. This work concentrates on investigating the peak transient loading conditions on a 30 mm cubic model submerged in the simulated downburst flow. The outflow induced pressures are recorded and compared to those from boundary layer and steady wall jet flow. Given that peak winds associated with downburst events are often located in the transient frontal region, the importance of using a non-stationary modelling technique for assessing peak downburst wind loads is highlighted with comparisons.

Keywords: thunderstorm; downburst; gust front; ring vortex loading; non-stationary loads.

1. Introduction and background

Thunderstorm downbursts are important for structural engineers because they produce the design wind speeds for mid to high return periods in many parts of the world (Holmes 2002, Twisdale and Vickery 1992). However, current structural design standards (Australia/New Zealand 2002, American Standard ASCE 7-05) only require design for pressures induced by an atmospheric boundary layer (ABL) flow. The ABL assumption is however inaccurate when considering the complex structure of a thunderstorm outflow (Mason, *et al.* 2005), and the ensuing wind loading conditions. For this reason it is not only important to model the flow field of thunderstorm downbursts, but also to determine the loading induced on typical structures by this type of wind event.

A downburst occurs when a strong downdraft impinges the ground and induces an outburst of straight or curved winds (likened to the divergence of an impinging jet) of damage causing intensity

* Professor, Corresponding Author, E-mail: darryl.james@ttu.edu

(Fujita 1990). Downbursts can be driven by precipitation drag, evaporative cooling, cloud and rain water melting, or a combination of these and other atmospheric processes.

In recent years, realizing the significance of downburst wind loading of structures, engineers have begun to develop wind loading models (Holmes 1992, Selvam and Holmes 1992, Wood, *et al.* 2001, Chay and Letchford 2002, Letchford and Chay 2002, Kim and Hangan 2007). Initial models used either stationary or moving, steady flow impinging jets, which were shown to give a relatively good representation of mean flow characteristics (Hjelmfelt 1988). Steady flow models, however, fail to simulate the transient vortex structure at the leading edge of the diverging outflow, a region known to be responsible for high wind speeds (Fujita 1985, Alahyari and Longmire 1995). Recently, transient simulations have begun to address this problem (Mason, *et al.* 2005, Kim and Hangan 2007, Lin, *et al.* 2007, McConville, *et al.* 2007), but to date little published research has surfaced on the loading ramifications of a transient front's movement over a structure. Initial investigations by one of the authors (Mason and Wood 2004), and a numerical investigation of potential loading by Kim, *et al.* 2007 have however been conducted and indicate that downburst wind loading may exceed design loading obtained from ABL winds.

From meteorological data, an idealized wind field model has been developed for a stationary downburst (Wilson, *et al.* 1984, Fujita 1985, Hjelmfelt 1988). Fig. 1 shows the main characteristics of the first few minutes (Wilson, *et al.* 1984) of an intense outflow life cycle. The downburst itself, prior to ground impact is made up of a single downdraft of colder more dense air with a leading edge circulation developed due to the shear layer between the colder descending air and the warmer surrounding atmospheric air. Once the downdraft impacts the surface the air turns radially outward beginning the formation of a wall jet. This wall jet is led by an expanding ring vortex. This outflow

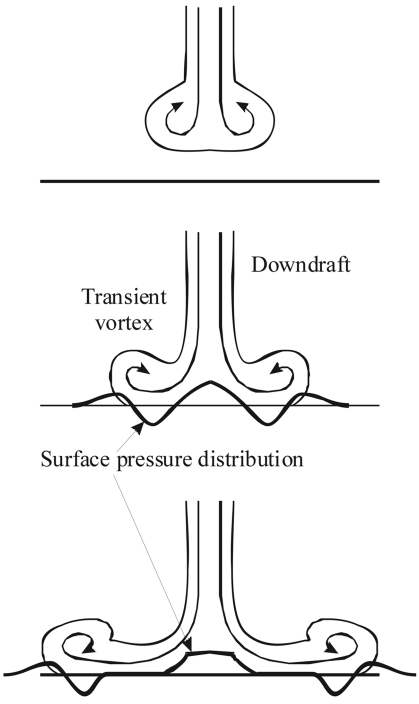

Fig. 1 Idealised stationary pulsed downburst flow field

description is to an extent idealised and may differ in the presence of environmental factors such as pre-existing wind shear, or storm translation.

The theorized surface pressure field associated with the translation of a horizontal vortex is also shown in Fig. 1 and conforms with surface pressure measurements made by Fujita (1985) and Bedard and Caplan (1987) for transient microburst fronts. The pressure is shown to be positive beneath the downdraft, forming a stagnation region directly at its centre. The pressure then decreases to a negative peak below the vortex core due to highly accelerated flow in that region. A positive pressure region travels ahead of this low-pressure due to stagnation of air in front of the travelling vortex. This transient surface pressure means that choice of a suitable reference pressure is an important consideration when analyzing wind-induced pressures on building models (Chay and Letchford 2002).

The purpose of the work presented in this paper is to evaluate the transient wind pressures on a cubic model subjected to the gust front of a simulated downburst. The physical downburst simulator of Mason, *et al.* (2005) was used to simulate the flow field, and the induced pressures were studied on a 30 mm cube. Measured pressure are normalised in a number of ways and compared to those measured with the same model in steady wall jet and boundary layer flows.

The following section discusses the experimental setup and procedures used for the cases presented in this paper. Section 3 describes the structure of the simulated downburst, while Section 4 presents the measured pressure distributions with emphasis on the leading ring vortex impact on the cubic model at various radial positions. Section 5 presents a discussion of the results and draws some conclusions on the significance of this work.

2. Experimental setup and procedure

The pulsed impinging jet used for the simulation of downburst-like flow in this study is fully described in Mason, *et al.* (2005), but for convenience is summarised here. The mean steady jet characteristics and model geometric configuration is given in Table 1. Fig. 2 shows the experimental setup with the variable cube location ($0.75 \leq X/D \leq 1.5$), and the pitot-static reference position indicated. The jet itself is inverted (blowing up) and was pulsed at the outlet by an aperture mechanism so the desired ring vortex would develop at the leading edge of the flow. The aperture itself is made up of 16 sheet metal blades pinned between a static base board and a rotational upper board. The mechanism behaves in a similar manner to a camera iris and rotation of approximately 10° allowed full opening or closing of the aperture. Aperture opening time was approximately 0.2 seconds; this however was shown to be too slow to avoid the aperture influencing the structure of the burst front produced. It was found that for the period of aperture opening the mechanism acted as a funnel and accelerated the flow leaving the jet outlet to a mean velocity larger than the steady flow value. Also, because the burst front was developed based as the aperture was expanding, the jet diameter D is not strictly representative for this initial region of flow. Despite this, the aperture

Table 1 Impinging jet steady flow characteristics

Jet Diameter (D)	0.51 m
Reference position	0.5D above jet outlet (0.255 m)
Reference velocity (V_j)	≈ 9 m/s ($Re_D \approx 3 \times 10^5$)
Centreline turbulence intensity	2%-4%
Jet outlet to test surface	1.7D (0.86 m)

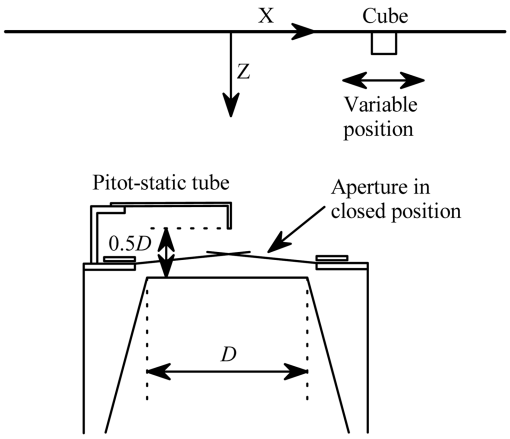

Fig. 2 Experimental setup of downburst simulation

successfully produced a vortex ring at the leading edge of the flow field and was therefore considered a successful simulation of a possible downburst type outflow event. The implications of the aperture limitations are discussed further later in this paper.

The length scale of 1/3000 (based on direct length scaling of an assumed full-scale downdraft diameter of 1.5 km) used in Mason, *et al.* (2005) is again applied here, and the 30 mm model cube represents a full-scale structure of approximately 90 m side dimension. The 1/3000 length scale should be viewed as simply an approximation given that downdrafts can range in dimension from a few hundred metres to several kilometres in diameter. A velocity scale of 1/3 and therefore a time scale of 1/1000 are also considered to be reasonable approximations based on the results of Mason, *et al.* (2005) and Fujita (1985).

Both steady flow and pulsed flow induced pressures were recorded with a Scanivalve DSM 3000 system and ZOC 33/64PX electronic pressure scanning module at 300 Hz. The model cube centerline was pressure tapped with 6 taps on the windward and leeward faces, 7 taps on the top face and 6 taps at mid height on one side face. 200 mm long, 1 mm internal diameter tubing with frequency response calculated to have a dynamic amplitude magnification of 3% at 50 Hz and ~9% at 100 Hz (Mason 2003) connected the pressure taps to the Scanivalve.

A pitot-static tube was mounted on a stand attached to the aperture base plate to measure a steady-state reference dynamic pressure for all tests. Atmospheric pressure in the laboratory provided a reference pressure for the transducers. A second reference velocity measurement was taken with a hot film probe, using a constant temperature anemometer system (TSI IFA300), positioned at the model eaves height ($z = 30$ mm) and located equidistant from the impinging jet centreline, but 200 mm away from the model so as to eliminate interference. This second velocity measurement was used to provide a transient eaves height reference dynamic pressure. All velocity measurements were also sampled at 300 Hz.

The induced pressures on the cubic model and the equivalent eaves height velocity were both recorded for 10 seconds per run. Within the first second the transient part of the test was recorded, while the remaining portion recorded the steady characteristics. Five repeat tests were made at each radial position, allowing peak-ensemble averaging of the initial transient and steady states flows to determine the pressure field characteristics. All pressure coefficient values given in this paper were determined to have an uncertainty of approximately ± 5%. These coefficient uncertainties were estimated assuming a constant pressure existed over each small area associated with a given tap using the method of Kline and McClintock (1953).

3. Flow field

Mason, *et al.* (2005) reported details of the simulated downburst wind field produced using the pulsed jet simulator. However, to aid in the understanding of the loading results presented in this paper, a brief discussion of the flow field is described.

The physical structure of the wind field impacting the model cube is made up of two parts. The first part being the initial non-stationary flow due to the pulsing of the jet, or in atmospheric terms, the gust front, and the second is the stationary field due to the steady impinging jet. The non-stationary component is made up of a succession of vortices with intermediate turbulent flow between them. The model cube first experiences what is termed the primary vortex, which is produced due to the flow instability occurring at aperture opening. Passage of this vortex is followed by an intermediate flow region that precedes the passage of a larger trailing vortex. The latter vortex was seen to be due to a combination of aperture effects and the natural shedding frequency of the jet. The trailing vortex is produced primarily as a side effect of the experimental setup (i.e., shedding); it is not known to what extent this trailing vortex would exist in a true downburst event. After the non-stationary component of flow, the cube experiences a succession of smaller vortices fed by the shear layer shed from the jet outlet. This flow characteristic has previously been documented in steady impinging wall jet flow (see for example Popiel 1991, Zaman and Husain 1980). In this paper however, it is the non-stationary region of the flow that is of interest.

The most important characteristics of the wind field for this particular experiment are the vertical (z) profiles of the surface parallel velocity, Fig. 3. For each elevation the peak velocity corresponding to the passage of the primary vortex was averaged over the five individual test runs to provide the profile shown. Mean velocities associated with the steady flow region are also shown. Velocities are shown normalised against the mean jet centre line velocity, V_j, while elevations are normalised against the jet diameter, D. The peak values represent something of an envelope of velocities associated with the vortex, and do not represent instantaneous structure. Steady flow profiles are shown as an

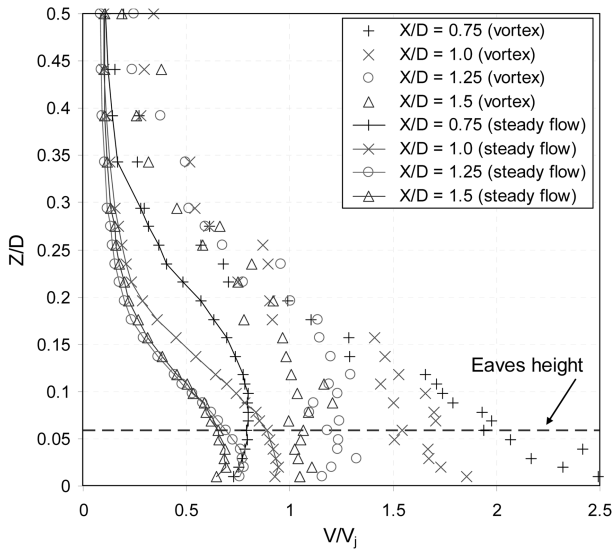

Fig. 3 Steady flow mean, and ensemble-averaged peak velocity (within the vortex) profiles at selected radial locations

indication of the difference between the velocity profile shapes for the stationary and non-stationary regimes, but again, are not the primary focus of this paper. For a detailed analysis of loading in the steady flow regime refer to Chay and Letchford (2002). Indicated on Fig. 3 is also the model eaves height elevation. It is seen that for almost all profiles the velocity maxima typically occur below the eaves height of the model. This is in stark contrast to what would be expected for a logarithmically increasing boundary layer flow. The instantaneous lateral horizontal profile of the front was shown in Mason, *et al.* (2005) to be practically constant over the width of the model cube suggesting a well-correlated lateral peak velocity profile.

4. Results and discussion

Pressure coefficients due to the passage of the primary vortex over the model are reported and discussed in this section. Two referencing procedures are explored in an attempt to collapse these data and enable comparison to similar results in boundary layer flow.

Induced pressure results are initially investigated normalised against the dynamic pressure defined by the mean jet outlet velocity, V_j. This is done so that an appreciation of the rapidly varying intensity of the vortex induced loads, as well as an indication of the structure of these loads can be gained. Time is normalised using the dimensionless time parameter t^*, and is defined in terms of the mean propagation velocity of the gust front, Vg_{prop}, time, t, and the jet exit diameter, D, Eq. (2). The mean gust front propagation velocity (Vg_{prop}) was determined by measuring the propagation speed of the primary vortex core utilizing a pulsed arc lamp that produced a plane of light pulsed at a fixed frequency for which helium filled soap bubbles streaks were recorded.

$$C_{Pj}(t) = \frac{P_{tap}(t) - P_{ATMOS}}{\frac{1}{2}\rho V_J^2} \tag{1}$$

$$t^* = \frac{t \cdot Vg_{prop}}{D} \tag{2}$$

4.1. Pressure time histories

Fig. 4 displays recorded time histories for four face representative taps. The five individual test runs are given so an indication of the test repeatability can be observed, with an ensemble average shown to highlight general trends. The locations of the pressure taps shown in Fig. 4 are highlighted on the inset cube diagram.

The transient pressure time histories shown in Fig. 4 were recorded with the model at X/D = 0.75, where the highest vortex induced winds speeds were observed (Fig. 3). Fig. 4(a) shows the time history for the windward face, and a clear peak is observed at $t^* \approx 0.3$ due to the passage of the primary vortex over the model. Normalised pressures peak in several cases at $Cp_j > 4$ producing magnitudes much higher than the steady flow pressure coefficient peaks that are observed for $t^* > 2.0$. The extremely high Cp_j values are in part due to a funnelling of air that occurs as the experimental aperture is being opened. As discussed in Section 2, this implies that for the gust front region (i.e., the region of flow influenced by aperture operation) V_j is an underestimate of the jet velocity. Given that only the influence of the frontal region is being studied, this underestimate is not an issue for comparison within this test, but it does mean that direct magnitude comparisons to

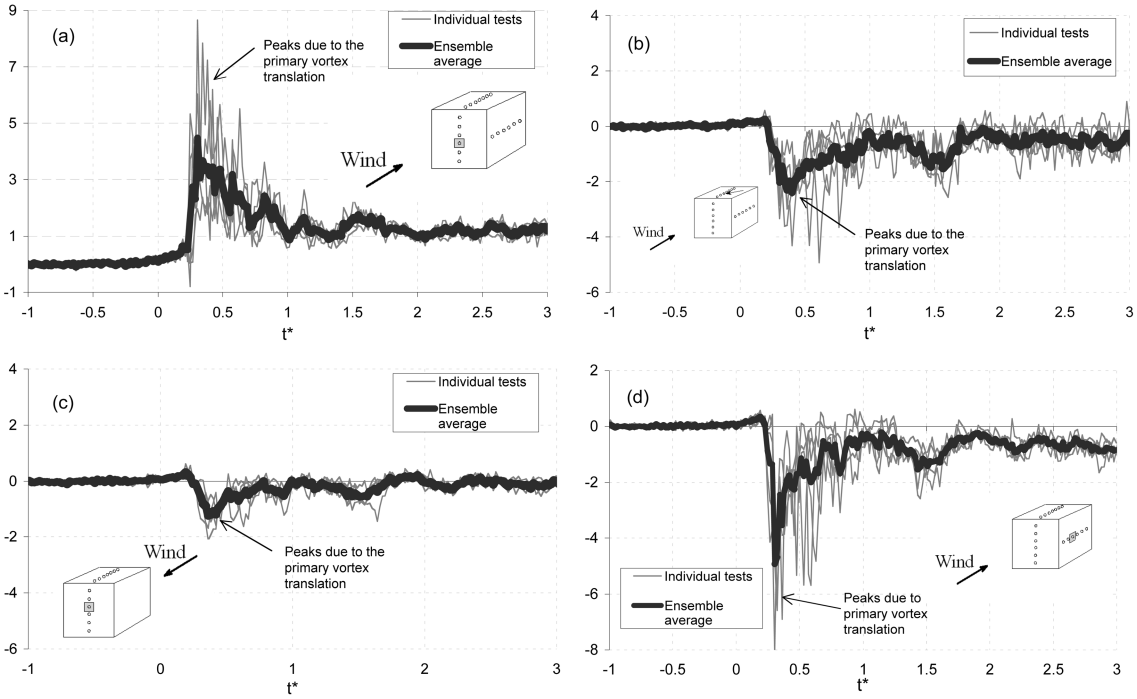

Fig. 4 Pressure coefficients for individual tests and ensemble averaged time histories for pressures measured at X/D = 0.75 for (a) the windward face, (b) the top face, (c) the leeward face, and (d) the side face

previous tests (e.g., Chay and Letchford 2002) based on this normalisation technique should not be made. A small second peak is seen at approximately $t^* = 1.5$ and this pressure peak is associated with the passage of the trailing vortex. The region between these peaks is highly turbulent and although a correlation between events can be seen in the moving mean sense, the actual correlation of individual peaks is quite poor. A brief negative pressure fluctuation was often observed just prior to the arrival of the primary vortex ($t^* = 0.25$), this is believed to be due to a draw up of air by the shear layer between the ambient air and the translating vortex.

Fig. 4(b) shows the transient time history for the top face, and it is observed that a sharp decrease in pressure to a suction peak is followed by a steady increase back to near zero with a second suction peak again around $t^* = 1.5$. As with the windward face the first peak is associated with the passage of the primary vortex while the second smaller peak is associated with the passage of the trailing vortex. It should be noted that for the top face, and indeed all faces, the ratio between primary and trailing peaks change quite significantly with radial position of the model. It was observed in Mason (2003) that the larger the radial distance (up to X/D = 1.75), the smaller the ratio of primary to trailing peak became. The magnitude of peak suction shown for the top face was approximately half the absolute magnitude of the peak positive pressure on the windward face. This is unlike loading from a typical boundary layer (Richards, *et al.* 2000) and is largely due to the velocity at eaves height being less than at the elevation shown in Fig. 4(a). This highlights a difficulty in designing structures for downburst winds using typical atmospheric boundary layer methods.

Fig. 4(c) shows the pressure time history recorded on the leeward face and as expected is of smaller magnitude than the top face due to its position in the developing wake region. The time

history however still exhibits the two distinct negative peaks due to the passage of the primary and trailing vortices. The short temporal separation between the windward and leeward face peaks suggests that these negative peaks can add to the overall maximum drag applied to the model. In full-scale though, this will depend on the length ratio between the vortex and loaded structure.

The transient pressure time history shown for the side face, Fig. 4(d), unlike what would be expected in a boundary layer flow, shows a larger peak pressure coefficient (at the same distance from the leading edge) than the top face. This is again likely due to the fact that the velocity profile reaches a maximum below eaves height for the simulated downburst winds. Largest suctions occur during the primary vortex passage with smaller peaks occurring during the trailing vortex. Suction peaks as large as $Cp_j = -8$ are observed for individual tests with good temporal correlation of peaks leading to an ensemble average peak of $Cp_j = -5.0$. It is evident however that the ratios of peak pressure coefficient measured on the windward, top, and side wall will vary depending on the height of the structure with respect to the elevation of peak velocity and the gradient of decay above and below this elevation at the point of loading. This again leads to issues when attempting to codify loading due to these types of wind events.

4.2. Pressure coefficient profiles

Extracting data from all measured pressure taps, Fig. 5 shows the centreline distribution of the normalised maximum averaged peak pressures as a function of radial position (X/D). Peak pressures were determined by finding the peak recorded pressure induced by the primary vortex at each discrete tap for each individual test, and then averaging those values over all runs. Pressure distributions are plotted against a developed centre line coordinate normalised by the height of the cube. The developed centreline coordinates runs over the model with windward, top and leeward faces presented as, 0-1, 1-2, and 2-3, respectively. Side face pressures are plot in the range 3-4.

It was shown in Fig. 4 that for $X/D = 0.75$ the largest overall peak pressures were due to the passage of the primary vortex. However, this was not the case for all radial positions. The larger size of the trailing vortex, and the rapid decay of the primary vortex (Mason, *et al.* 2005), meant that for radial positions $X/D \geq 1.25$, individual trailing vortex peaks were sometimes larger than their primary vortex counterparts. These trailing peak have however not been considered here as the primary concern is the loading due to the leading vortex and to document how this changed with divergence.

As expected, Fig. 3, the radial position $X/D = 0.75$ produced the largest magnitude pressures on all faces. For the windward face the largest pressures occur at cube mid-height for all radial positions. The ratio of pressures recorded at the centre of the windward face to those measured at the top and bottom of this face decreases with increasing radial distance from the jet. This change in ratio is anticipated when considering that with divergence the average peak velocity profiles become more uniform with height (Fig. 3). The fact that the lower taps give lower pressures departs from the peak velocity profile that shows the largest average peak velocity at 5 mm ($Z/D = 0.17$) (between the first and second tap). The reason for this is likely due to a developing recirculation region in front of the cube, a feature that is present in most surface mounted bluff body flow.

The top face again shows a decrease in pressure magnitude with an increase in radial distance from the impinging jet. All profiles are similar in shape with the averaged maximum pressures occurring at either the second or third tap from the leading edge. Fig. 5 also shows that the observation made earlier regarding the peak magnitude ratio between the front and top faces is repeated for all radial

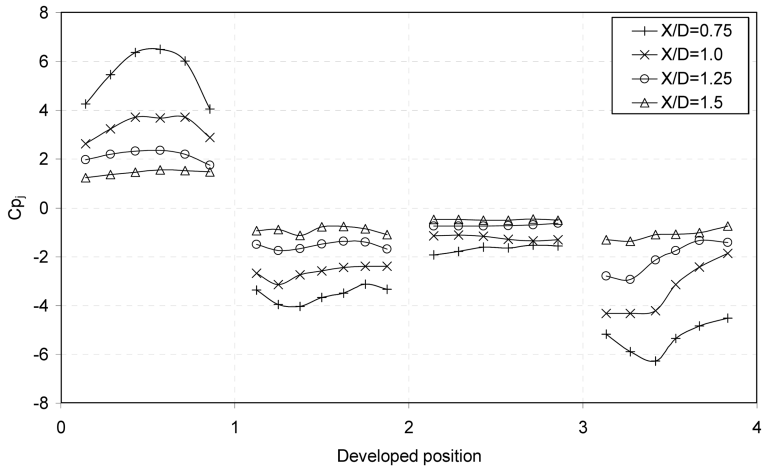

Fig. 5 Averaged normalised maximum pressure coefficients along the, windward (0-1), top (1-2), leeward faces (2-3), and side face (3-4) of the cube referenced to jet reference dynamic pressure

locations. The ratio does however decrease with an increase in radial position as expected due to the more uniform velocity profile. The lee face profile shape is as would be expected and also displays a decrease in magnitude with increased radial distance from the jet.

On the side face, Fig. 5, for X/D = 0.75, a distinct peak at the third tap back from the leading edge exists. The shape of this profile is more what would be expected on a bluff body wall, unlike the flatter profile shown for the top face. It is speculated that this difference is because the unconfined nature of the wall flow (vertically) means that the flow is not accelerated over the model in the same way as normally expected. The flow over the side wall however is essentially still bounded in a similar fashion as in boundary layer flow.

In an attempt to remove the variability in Cp_j magnitude observed in Fig. 5, pressure coefficients were recalculated ($Cp_{e\text{-}transient}$) using a transient eaves height based reference velocity, $V_{eaves}(t)$, in lieu of V_j used in Eq. (1). This normalisation process includes localised (temporally and spatially) velocities measured at the same radial distance from the jet centreline in the pressure coefficient denominator. A temporal filter was also applied to the data (both pressures and velocities) to remove small scale fluctuations about the transient mean not likely to be correlated between the cube and reference positions. A 7 point (0.0233 second) moving average was chosen to smooth both the velocity and pressure time histories. This filtration process is similar to that employed by Holmes, *et al.* (2008) and Choi (2004) for analysis of full-scale outflow events, and the scaled filtration time of approximately 25 seconds (a time scale of 1/1000 is used) is of similar order to the 40 seconds used by Holmes, *et al.* (2008). Therefore $Cp_{e\text{-}transient}(t)$ becomes akin to a pseudo-static pressure coefficient based on smoothed $V_{eaves}(t)$ and $P_{tap}(t)$ time histories. This filtration process also means that a direct comparison to pressure coefficients previously measured in steady state wall jet, and boundary layer simulations or experiments can be made (no allowance has been made for differing averaging periods, e.g. Durst 1960). After this initial data filtration, a second filtering process was implemented allowing only Cp values with an actual pressure magnitude greater than $|\max(P_{tap}(t))/2|$ to be used. This was done so that low magnitude pressure data would be excluded from the analysis, where it was possible that a low local velocity could lead to a large but irrelevant pressure coefficient. Pressure coefficients based on this new normalisation process yielded a much

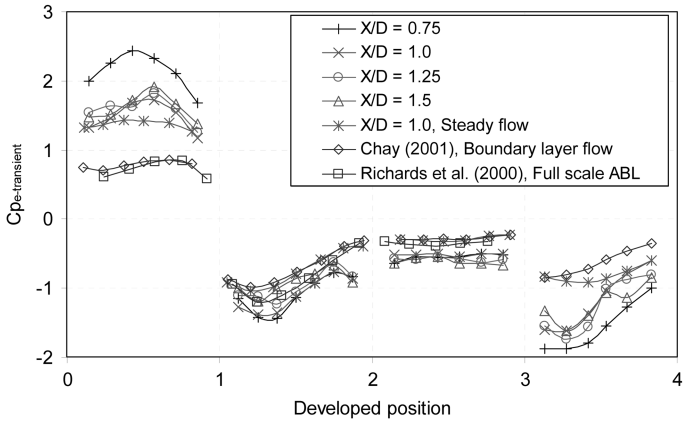

Fig. 6 Transient dynamic pressure coefficients along the, windward, top, leeward and, side faces of the model cube. Developed positions are as in Fig. 5

cleaner collapse of the data for $X/D \geq 1$ as shown in Fig. 6.

The profiles shown in Fig. 6 take on the same form as those in Fig. 5, but referencing them to a localised (space and time) and averaged velocity facilitates a better collapse of data. For radial positions $0.75 \leq X/D \leq 1.5$ the collapse is quite good for all faces, with the only deviations occurring on the windward, and to a lesser extent, side face for the radial position $X/D = 0.75$. Invoking the quasi-steady assumption, the disparity at this radial position can be partially explained with the aid of peak velocity profiles shown in Fig. 3. For the region below model eaves height the profile of velocities for radial positions $X/D \geq 1.0$ were fairly similar in shape, but for $X/D = 0.75$ there is a much sharper decrease in velocity with height. However, simply using this method suggest that a value of $Cp_{e\text{-transient}}$ equal to approximately 1.5 should be obtained for the windward face at $X/D = 0.75$. The reason larger values exist is because the peaks in the pressure time histories were often seen to lag the eaves height velocity, thus leading to a situation where the peak pressure is not normalised by the peak velocity. This small lag was also evident in a series of instantaneously acquired velocity measurements over a range of heights in Mason (2003). Note however that even though an averaging process has been implemented the time histories still displayed a rapidly varying mean, thus a lag of only a time step or two had significant implications for the pressure coefficient.

Along side measured pressure coefficients are those measured in boundary layer (Chay 2001 (simulation), Richards, *et al.* 2001 (full-scale)), and steady wall jet simulations. The boundary layer flow results of Chay (2001) were measured using the same cubic model in a boundary layer wind tunnel with velocity and turbulence structure equivalent to a scaled design Category 1 wind (Standards Australia 2002). The full scale results of Richards, *et al.* (2000) are based on measurements taken on the Silsoe cube in a grassed field. For all faces the magnitude of the boundary layer induced pressures are noticeably less than the simulated downburst winds. This is particularly clear on the windward face where pressures are most significantly driven by the approach velocity profile. The primary reason for this is that the reference velocity for the pulsed impinging jet simulations is lower than the velocities that influence the loading of the model, unlike for the boundary layer cases where the relationship is reversed. The similar profile shapes indicate that despite the current simulations non-stationary nature, and differing loading velocity profile, the bluff-body reaction to the winds is relatively comparable. Steady impinging jet results also appear to be similar in shape and magnitude to those of the current test on the windward face, but more closely approximate the

mean boundary layer results on the top, lee and side faces.

5. Conclusions

A pulsed impinging jet was used to simulate the leading edge of a stationary thunderstorm downburst outflow. The effects of this simulated downburst flow field on a model cube were studied. The induced pressures were shown referenced to both a steady jet outflow velocity and a filtered transient eaves height velocity. The jet referenced data allowed a relative comparison of pressure magnitudes at different radial positions to be made, while a local (in space and time) but transient eaves height reference dynamic pressure was sought to collapse the data. The eaves height referenced data were also filtered so that moving mean pressure distributions could be assessed and compared to boundary layer and impinging jet results. The jet referenced data showed that as with the velocities, the largest loading occurred nearest to the jet impingement with a steady decrease in magnitude with increasing distance from this position. Profile shapes were shown to be reasonably similar on the top and lee faces but significantly varied with radial position for the windward and side faces. The eaves height referenced data collapsed well for the region $1.0 \leq X/D \leq 1.5$, with only a shift in magnitude for $X/D = 0.75$. The reason for the different profile magnitudes was attributed to the variable velocity gradients at the different locations, and the variable lag between peaks at different locations on the model. The shapes of the loading profiles, particularly on the windward and side faces, were shown to be similar but not identical to those induced by simulated boundary layer winds. It was also found that the building length could potentially play a role in determining the instantaneous loading because localised gusts may not be correlated between the windward and lee faces of a structure. This however will be dependent on the vortex/structure size ratio.

Acknowledgements

This work was undertaken on a Texas Higher Education Advanced Research Project. The recommendations of the reviewers significantly contributed to the final layout of this paper and are greatly acknowledged.

References

Alahyari, A. and Longmire, E.K. (1995), "Dynamics of experimentally simulated microbursts", *AIAA J.*, **33**(11), 2128-2136.

American Society of Civil Engineers (2005), *Minimum design loads for buildings and other structures*, ASCE Standard, ASCE/SEI 7-05, American Society of Civil Engineers, New York.

Bedard, A.J. and Caplan, S.J. (1987), "Microburst vorticity", *25th Aerospace Science Meeting*, American Institute of Aeronautics and Astronautics, Reno.

Chay, M.T. (2001), "Simulation of thunderstorm downbursts", MSCE Thesis, Texas Tech University.

Chay, M.T. and Letchford, C.W. (2002), "Pressure distributions on a cube in a simulated thunderstorm downburst, Part A: Stationary downburst observations", *J. Wind Eng. Ind. Aerod.*, **90**, 711-732.

Durst, C.S. (1960), "Wind speeds over short periods of time", *Meteorol. Mag.*, **89**, 181-186.

Forbes, G.S. and Wakimoto, R.M. (1983), "A concentrated outbreak of tornadoes, downbursts and microbursts, and implications regarding vortex classification", *Monthly Weather Review*, **111**, 220-235.

Fujita, T.T. (1981), "Tornadoes and downbursts in generalized planetary scales", *J. Atmos. Sci.*, **38**, 1511-1534.

Fujita, T.T. (1985), *Downburst: Microburst and macroburst*, Univ. of Chicago Press, Chicago, Illinois.

Fujita, T.T. (1990), "Downbursts: meteorological features and wind field characteristics", *J. Wind Eng. Ind. Aerod.*, **36**, 75-86.

Hjelmfelt, M.R. (1988), "Structure and life cycle of microburst outflows observed in Colorado", *J. Appl. Meteorol*., **27**, 900-927.
Holmes, J.D. (1992), "Physical modeling of thunderstorm downdrafts by wind-tunnel jet", *2nd Australasian Wind Engineering Society Workshop on Wind Engineering*, Melbourne, February 20-21.
Holmes, J.D. (2002), "A re-analysis of record extreme wind speeds in region A", *Aust. J. Struct. Eng*., **4**, 29-40.
Kim, J.D. and Hangan, H.M. (2007), "Numerical characterization of impinging jets with application to downbursts", *J. Wind Eng. Ind. Aerod.*, **95**, 279-298.
Kim, J.D., Hangan, H.M. and Ho, T.C.E. (2007), "Downbursts versus boundary layer induced wind loads for tall buildings", *Wind Struc*., **10**, 481-494.
Kline, S.J. and McClintock, F.A. (1953), "Describing Uncertainties in Single-sample Experiments", *Mech. Eng.*, **75**, 3.
Letchford, C.W. and Chay, M.T. (2002), "Pressure distributions on a cube in a simulated thunderstorm downburst, Part B: Moving Downburst Observations", *J. Wind Eng. Ind. Aerod.*, **90**, 733-753.
Lin, E.W., Orf, L.G., Savory, E. and Novacco, C. (2007), "Proposed large-scale modelling of the transient features of a downburst outflow", *Wind Struc.*, **10**, 315-346.
Lundgren, T.S., Yao, J. and Mansour, N.N. (1992), "Microburst modelling and scaling", *J. Fluid Mech.*, **239**, 461-488.
Mason, M.S. (2003), "Pulsed jet simulation of thunderstorm downbursts", MSCE Thesis, Civil Engineering, Texas Tech University.
Mason, M.S. and Wood, G.S. (2004), "Loading of a very tall building in a simulated downburst wind field", *Proc. of 11th Australasian Wind Engineering Society Workshop*, Darwin, Australia.
Mason, M.S., Letchford, C.W. and James, D.L. (2005), "Pulsed wall jet simulation of a stationary thunderstorm downburst, Part A: Physical structure and flow field characterization", *J. Wind Eng. Ind. Aerod.*, **93**, 557-580.
McConville, A., Sterling, M. and Baker, C. (2007), "An introduction of the scaling issues associated with the physical simulation of thunderstorm downbursts", *Proc. 12th Int. Conf. on Wind Engineering*, 1431-1438, Cairns.
Popiel, C.O. and Trass, O. (1991), "Visualization of a free and impinging round jet", *Exp. Therm. Fluid Sci.*, **4**, 253-264.
Proctor, F.H. (1988), "Numerical simulations of an isolated microburst, Part 1: Dynamics and Structure", *J. Atmos. Sci.*, **45**, 3137-3159.
Richards, P., Hoxey, R.P. and Short, L.J. (2000), "Wind pressures on a 6m cube", *Fourth International Colloquium on Bluff Body Aerodynamics and Applications*, Ruhr University, Bochum, Germany, 515-518.
Standards Australia (2002), *Structural design actions*, *Part 2: Wind actions,* Standards Australia, Sydney, NSW, Australia.
Selvam, R.P. and Holmes, J.D. (1992), "Numerical simulation of thunderstorm downdrafts", *J. Wind Eng. Ind. Aerod.*, **41-44**, 2817-2825.
Twisdale and Vickery, P.J. (1992), "Research on thunderstorm wind design parameters", *J. Wind Eng. Ind. Aerod.*, **41**, 545-556.
Wakimoto, R.M. (1982), "The life cycle of thunderstorm gust fronts as viewed with Doppler radar and rawinsonde data", *Monthly Weather Review*, **110**, 1060-1082.
Wilson, J.W., Rita, D.R., Kessinger, C. and McCarthy, J. (1984), "Microburst wind structure and evaluation of Doppler radar for airport wind shear detection", *J. Climate and Applied Meteorology,* **23**, 898-915.
Wood, G.S. and Kwok, K.C.S. (1998), "An empirically derived estimate for the mean velocity profile of a thunderstorm downdraft", *Proc. of the 7th Australasian Wind Engineering Society Workshop*, Auckland, N.Z.
Wood, G.S., Kwok, K.C.S., Motteram, N.A. and Fletcher, D.F. (2001), "Physical and numerical modeling of thunderstorm downbursts", *J. Wind Eng. Ind. Aerod.*, **89**, 535-552.
Yao, J. and Lundgren, T.S. (1996), "Experimental investigation of microbursts", *Exp. Fluids*, **21**, 17-25.
Zaman, K.B.M.Q. and Husain, A.K.M.F. (1980), "Vortex pairing in a circular jet under controlled excitation, Part 1: General jet response", *J. Fluid Mech.*, **101**, 449-491.

JH